

# The Role of the Intersection Space in the Photochemistry of Tricyclo[3.3.0.0<sup>2,6</sup>]octa-3,7-diene

Luis Manuel Frutos,<sup>\*,†</sup> Unai Sancho,<sup>†</sup> Marco Garavelli,<sup>‡</sup> Massimo Olivucci,<sup>§,||</sup> and Obis Castaño<sup>\*,†</sup>

Departamento de Química Física, Universidad de Alcalá, 28871 Alcalá de Henares (Madrid), Spain, Dipartimento di Chimica "G. Ciamician", Università di Bologna, Via Selmi 2, 40126 Bologna, Italy, Dipartimento di Chimica Organica, Università di Siena, Via Aldo Moro, 53100 Siena, Italy, and Chemistry Department, Bowling Green State University, Bowling Green, Ohio 43403

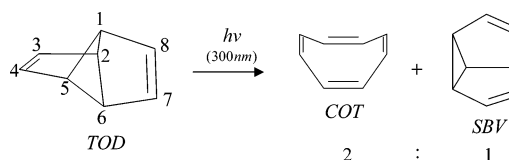
Received: November 15, 2006; In Final Form: January 14, 2007

CASSCF and CASPT2 methods were used to study the photochemistry of tricyclo[3.3.0.0<sup>2,6</sup>]octa-3,7-diene (TOD). The analysis of different S<sub>1</sub> reaction paths as well as the topology of the S<sub>1</sub>/S<sub>0</sub> intersection space allows us to establish two novel properties associated with the photochemical behavior of this compound: (i) simple low-lying intersection space domains can mediate different photoproducts, and (ii) TOD photochemistry is probably mediated by two disconnected intersection space domains, related to the formation of cyclooctatetraene and semibulvalene in different time-scales. It is shown that these domains are chemically distinct since the first, leading to COT, mediates barrierless pericyclic reactions while the second, leading to SBV, is accessed through the formation of an excited-state biradical intermediate. To the best of our knowledge, in the domain of single molecule photochemistry, TOD represents the first example where a different chemical role of distinct low-lying intersection spaces has been computationally documented. The observed photoproducts can be rationalized in terms of branching space diagrams, constructed by determining the branching space (derivative coupling and gradient difference vectors) for each conical intersection involved in the photochemical process.

Conical Intersections (CI) are fundamental mechanistic keys to understanding photochemical processes.<sup>1</sup> Usually, only one CI structure is considered when dealing with the mechanism of a photochemical reaction. Nevertheless, conical intersection points are elements of the intersection space: an N-2-dimensional subspace of conical intersections (where N corresponds to the vibrational degrees of freedom of the reacting system),<sup>2</sup> and consequently, full segments of this subspace can be involved in the decay process.<sup>3</sup> The segment of the intersection space accessible by the system are likely to be "chemically homogeneous" (i.e., photoproducts originating from all the points of the segment are the same), nevertheless, in principle, it may be possible that a finite intersection space segment provides different reaction channels leading to different photoproducts.<sup>1(b),3</sup>

In this work we present an investigation of the photochemistry of tricyclo[3.3.0.0<sup>2,6</sup>]octa-3,7-diene (TOD, see Scheme 1) and provide evidence in favor of the existence of two chemically distinct intersection spaces S<sub>1</sub>/S<sub>0</sub> involved in the decay process. Furthermore, we show that the distinct accessibility of these intersection spaces leads to complex photochemical behavior, where the different photoproducts (semibulvalene, SBV and 1,3,5,7-cyclooctatetraene, COT) are formed on different time-scales because of the different paths followed (i.e., activationless for COT and through an intermediate for SBV) in the relaxation process on the excited state (S<sub>1</sub>).

## SCHEME 1: TOD Ground State Equilibrium Structure (Numbering Used in the Text) and the Experimentally Observed Photoproducts: 1,3,5,7-Cyclooctatetraene (COT) and Semibulvalene (SBV) in Approximate Proportion of 2:1



Experimental results indicate that irradiation of TOD at  $-60\text{ }^{\circ}\text{C}$  leads to the concomitant formation of SBV and COT in an approximate ratio of 2:1 (See Scheme 1).<sup>4</sup> The low-temperature ensures that the isomerization of TOD to SBV is negligible in the time-scale of the complete photochemical reaction (i.e.,  $\sim 1\text{ h}$ ). Different mechanisms have been proposed for the photochemical rearrangement of TOD to yield COT and SBV, involving a [2+2] retro-cycloaddition for COT and a concerted suprafacial[1,3]-sigmatropic shift for SBV, or the formation of COT and SBV via a highly vibrationally excited biradical intermediate.<sup>4</sup> Nevertheless, none of the mechanisms have been validated by experimental or theoretical studies.

Our theoretical investigation gives, for the first time, an insight into the mechanism of the photoreaction. It is shown that COT is formed mainly via an efficient ultrafast internal conversion process (that may occur in the femtosecond time-scale) where decay to the ground state occurs through an intersection space domain comprising two qualitatively different mechanisms of reaction: a [2+2] cycloaddition for a  $D_2$  symmetry CI, and a photocyclization where a single  $\sigma$  transannular bond is formed/broken for a  $C_2$  symmetry CI. On the

\* Corresponding authors. E-mails: luisma.frutos@uah.es, obisd.castano@uah.es

<sup>†</sup> Universidad de Alcalá.

<sup>‡</sup> Università di Bologna.

<sup>§</sup> Università di Siena.

<sup>||</sup> Bowling Green State University.

**TABLE 1: CASSCF and CASPT2/6-31G(d) Energies for the Significant Points of the PES**

structure	CASSCF(8, 8)/6-31G(d) <sup>a</sup>		CASPT2(8, 8)/6-31G(d) <sup>a,b</sup>		relative energy <sup>c</sup>	
	S <sub>0</sub>	S <sub>1</sub>	S <sub>0</sub>	S <sub>1</sub>	S <sub>0</sub>	S <sub>1</sub>
TOD ( <i>D</i> <sub>2d</sub> ) <sup>d</sup>	-307.54377	-307.29416	-308.50927	-308.34153	0.00 (0.00)	156.63 (105.26)
TOD ( <i>D</i> <sub>2d</sub> ) <sup>e</sup>	-307.39934	-307.16461	-308.36484	-308.21198	0.00 (0.00)	147.29 (95.92)
<b>BR</b> ( <i>C</i> <sub>s</sub> )	-307.56744	-307.46165	-308.50755	-308.40039	-14.85 (1.08)	51.53 (68.32)
<b>BR</b> ( <i>C</i> <sub>s</sub> ) <sup>f</sup>	-307.56709	-307.45995	-308.50650	-308.40337	-14.63 (1.74)	52.60 (66.45)
<b>CI1</b> ( <i>D</i> <sub>2</sub> )	-307.45600	-307.45287	-308.41001	-308.40667	55.08 (62.28)	57.04 (64.38)
<b>CI2</b> ( <i>C</i> <sub>2</sub> )	-307.47763	-307.47674	-308.42460	-308.42830	41.50 (53.13)	42.06 (50.81)
<b>CI3</b> ( <i>C</i> <sub>1</sub> )	-307.47107	-307.47049	-308.42902	-308.42640	45.62 (50.36)	45.98 (52.00)
TS <sub>CI3</sub> ( <i>C</i> <sub>1</sub> )	-307.51152	-307.43703	-308.45885	-308.41163	20.24 (31.64)	66.98 (61.27)
TS <sub>CI3</sub> ( <i>C</i> <sub>1</sub> ) <sup>g</sup>	-307.53256	-307.44206	-308.47515	-308.39405	7.03 (21.41)	63.82 (72.30)
<b>CI4</b> ( <i>C</i> <sub>s</sub> )	-307.45837	-307.45830	-308.41248	-308.41098	53.59 (60.74)	53.63 (61.68)
TS <sub>CI4</sub> ( <i>C</i> <sub>s</sub> )	-307.54241	-307.45238	-308.48783	-308.39716	0.85 (13.45)	57.35 (70.35)
TS <sub>CI4</sub> ( <i>C</i> <sub>s</sub> ) <sup>h</sup>	-307.56467	-307.44971	-308.50259	-308.39032	-13.11 (4.19)	59.02 (74.64)
<b>CI5</b> ( <i>C</i> <sub>1</sub> )	-307.45205	-307.45188	-308.41332	-308.40634	57.55 (60.21)	57.66 (64.59)
TS <sub>CI5</sub> ( <i>C</i> <sub>1</sub> )	-307.49078	-307.45129	-308.45737	-308.40312	32.57 (40.81)	58.03 (66.61)
TS <sub>CI5</sub> ( <i>C</i> <sub>1</sub> ) <sup>i</sup>	-307.55377	-307.45008	-308.49951	-308.39450	6.27 (6.12)	58.79 (72.02)
<b>CI1</b> ( <i>C</i> <sub>2</sub> )	-307.48049	-307.48019	-308.42370	-308.42906	39.71 (53.69)	39.90 (50.33)
<b>CI1</b> ( <i>C</i> <sub>2v</sub> ) <sup>j</sup>	-307.52527	-307.51695	-308.44985	-308.46159	11.61 (37.29)	16.83 (29.92)

<sup>a</sup> Absolute energies in a.u. <sup>b</sup> CASPT2 eigenvalues were examined in order to eliminate contributions from intruder states (weight of the reference function > 0.74 in all cases). <sup>c</sup> Relative to TOD (*S*<sub>0</sub> equilibrium geometry) CASSCF energies in kcal/mol. The relative CASPT2 energies are given in parenthesis. <sup>d</sup> Oscillator strength for the *S*<sub>0</sub> → *S*<sub>1</sub> FC transition in TOD equal to 0.0851. <sup>e</sup> Electronic energies with zero point energy (ZPE) corrections obtained by CASSCF(8,8)/6-31G\* analytical frequencies. In this case relative energies are taken from the ZPE corrected energy on the ground state. <sup>f</sup> Optimized geometry at the CASPT2 with a CASSCF(6,6)/6-31G(d) reference wave function level. <sup>g</sup> Transition state structure at the CASPT2 level determined from the IRC at the CASSCF level is the corresponding higher energy point along the CASSCF IRC. <sup>h</sup> TS for the **CI4** determined by linear scan linking **BR** and **CI4** at the CASPT2 level of theory. <sup>i</sup> TS for the **CI5** determined by linear scan linking **BR** and **CI5** at the CASPT2 level of theory. <sup>j</sup> Absolute minimal energy conical intersection of the subspace. Data taken from ref 17b.

contrary, SBV is mainly formed via an *S*<sub>1</sub> intermediate biradical species, which can evolve rapidly (with low energy of activation) to reach a second intersection space domain, which provides an efficient funnel for radiationless decay to the ground state and SBV formation.

## Results and Discussion

**1. Photochemical Reaction Paths.** The singlet absorption spectrum of TOD, a nonconjugated diene hydrocarbon, shows specific behavior since it cannot be considered as the sum of the two isolated double bond spectra. As shown earlier,<sup>5</sup> hyperconjugation through the highly strained cyclobutane central ring, couples the double bonds, giving an *S*<sub>1</sub> excitation energy (~300 nm) lower than the corresponding *S*<sub>1</sub> band of two non-interacting double bonds (~250 nm).<sup>4</sup> This fact indicates that the  $\sigma$  molecular orbitals of the central cyclobutane ring must be enclosed in the active space of multiconfigurational calculations<sup>6</sup> (see also Computational Details) because of the role in the hyperconjugation. This is consistent with the computed CASPT2 *S*<sub>0</sub> → *S*<sub>1</sub> excitation energy (~272 nm, see Table 1). Zero-point vibrational energy correction leads to a more stabilized *S*<sub>1</sub> state (by ~9 kcal/mol), giving a *S*<sub>0</sub> → *S*<sub>1</sub> absorption wavelength (~298 nm) that is in very good agreement with the experiment. At the FC point, the *S*<sub>1</sub> potential energy curvature (second derivatives) presents five negative values, corresponding to vectors of *D*<sub>2</sub>, *C*<sub>2</sub>, *C*<sub>s</sub> (twofold degenerate) and *D*<sub>2</sub> symmetry, which are orthogonal to the energy gradient vector.<sup>7</sup>

These five negative eigenvalues of the Hessian also reveal that the initial relaxation directions from the FC point on *S*<sub>1</sub> can occur as a combination of five directions (apart of the energy gradient vector).<sup>8</sup> Accordingly, the possible initial relaxation directions from the FC point were searched by performing minimum energy path (MEP) computations starting from structures with a small initial distortion (0.03 amu<sup>1/2</sup> bohr) along the modes associated with the five negative curvatures. The results demonstrate that, initially, the computed MEPs are almost co-incident and lead to a common transient tetradicaloid structure corresponding to a bifurcation point, **BPI**, where the

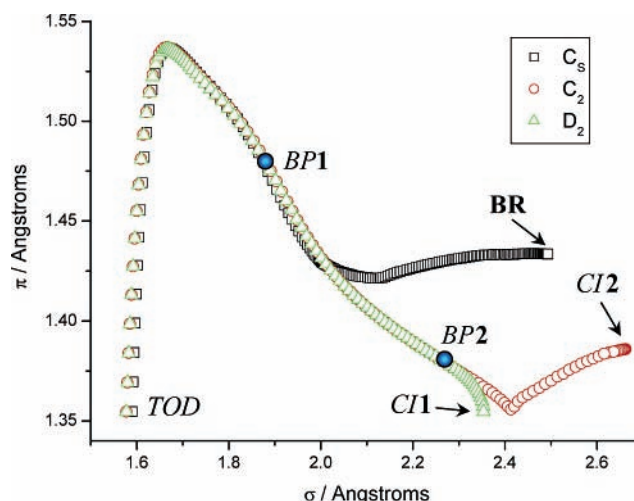


**Figure 1.** Plot of the three qualitatively different MEPs related to the relaxation processes after the *S*<sub>0</sub> → *S*<sub>1</sub> FC transition for TOD. The MEPs are displayed as a function of  $\sigma$  and  $\pi$  coordinates.<sup>9</sup> Two of the three MEP (those of symmetry *D*<sub>2</sub> and *C*<sub>2</sub>) finish in a Conical Intersection (CI 1 and 2 respectively), while the *C*<sub>s</sub> MEP finishes in a biradical species (**BR**). The three MEPs diverge due to the presence of two bifurcation points (**BPI** and **BP2** points) on *S*<sub>1</sub> (marked with blue circles).

two double bonds (*C*<sub>3</sub>=*C*<sub>4</sub> and *C*<sub>7</sub>=*C*<sub>8</sub>) are almost broken reaching a value for the CC distance of ~1.5 Å, which corresponds to a single bond (see Figure 1). The bifurcation points are characterized by a zero eigenvalue of the diagonal projected Hessian (see computational details). The formation of this unstable structure is also characterized by expansion of the CC  $\sigma$  bonds of the central strained cyclobutane ring, which provides a stabilization of the system by allowing a through bond coupling of the radical centers.<sup>5</sup>

Beyond **BPI**, we found that the MEPs with an initial distortion along the normal modes of symmetry *D*<sub>2</sub> and *C*<sub>2</sub>, reach two different CIs (**CI1** and **CI2** respectively) that provide efficient “funnels” connecting the excited-state to the ground state. We have used the properties of the first-order branching

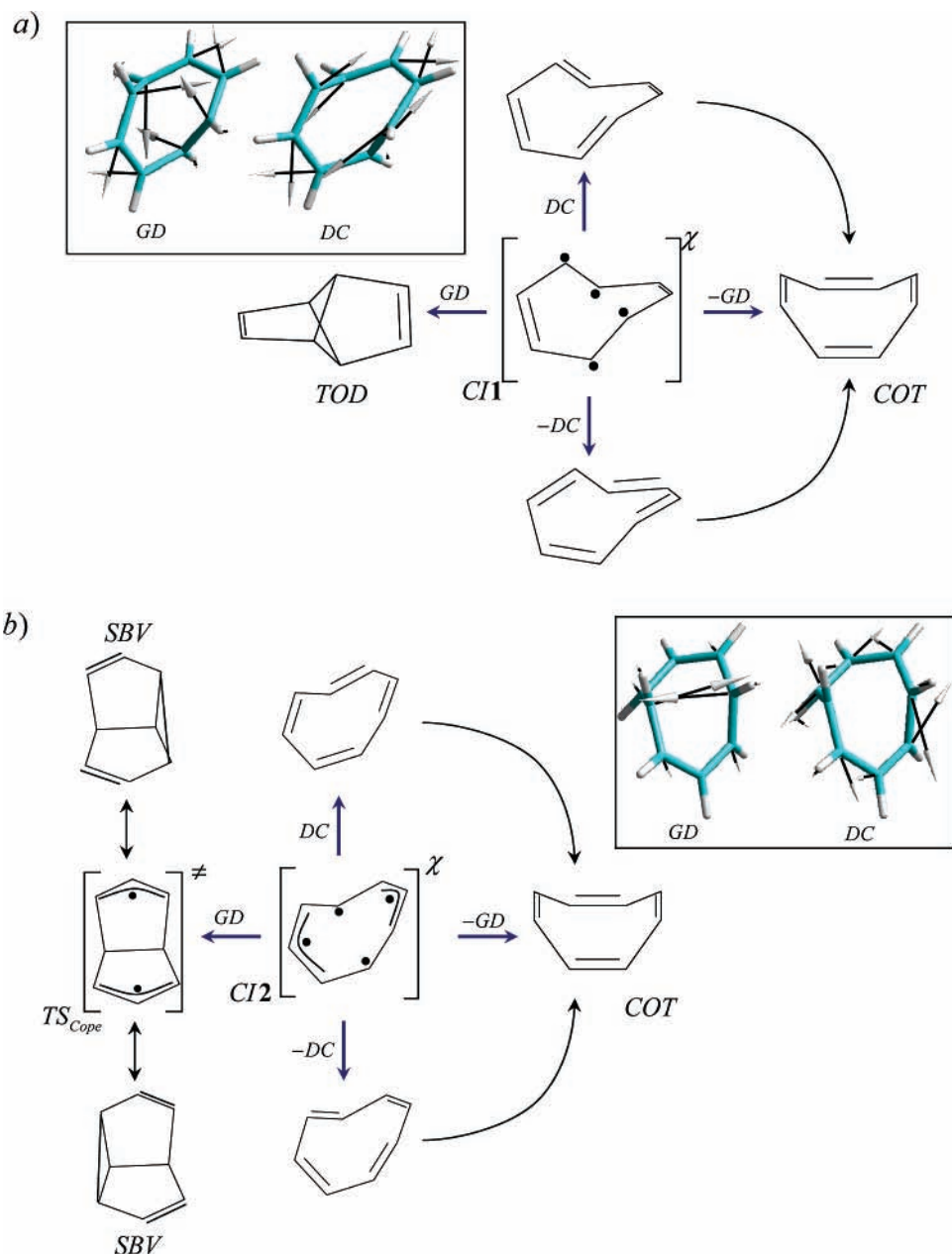


**Figure 2.** Branching space diagrams for CI1 of  $D_2$  symmetry (a) and CI2 of  $C_2$  symmetry (b) are shown. GD and DC vectors expands the two-dimensional branching space that lifts out the energy degeneracy. CI1 corresponds with a [2+2] cycloaddition (given by the GD vector), while CI2 is related with a radical photocyclization (GD vector). The DC vector stands by the  $\pi$ -charge coupling in both cases.

space, that is, the linear two-dimensional subspace of coordinates where the energy degeneracy is lifted, to characterize these conical intersections, i.e., to predict and rationalize the possible relaxation paths on  $S_0$  and consequently the possible formed photoproducts. The branching space diagrams for CI1 and CI2 are given in Figure 2.

These diagrams suggest that CI1 may mediate an intramolecular cycloreversion while CI2 may mediate a radical photocyclization. In order to confirm this prediction, we computed equally spaced MEPS in the branching space according to the prescriptions defined in ref 10. Different minima on  $S_0$ , associated with different photoproducts, were reached. Accordingly, from the CI1 ( $D_2$  symmetry), reversion to the reactant (TOD) as well as the formation of cyclooctatetraene (COT) was confirmed. On the other hand, from CI2 ( $C_2$  symmetry) the computed MEPS were consistent with the formation of COT as well as trans,cis,trans,cis-COT (t,t-COT)<sup>11</sup> (notice that the large value of the  $C_1$ – $C_2$  distance (2.39 Å) in CI2 is likely to be

responsible for the lack of a photocyclization product from this funnel; only when such a distortion is reduced (for example 2.11 Å in CI3, see below) the photocyclization may occur). Since no barriers were detected along either the  $S_1$  or  $S_0$  MEPS, the described photochemical pathways which involve decay at CI1 and CI2 must be related to ultrafast dynamics (i.e., no intermediate is populated in the excited-state and the decay to the ground state occurs via a CI) (see Figure 3).

CI1 and CI2 are qualitatively different in both the geometrical structure of the conical intersections and the structure of the branching space. These changes are obviously enough to prompt the formation of different photoproducts. As seen above, already the analysis of the derivative coupling (DC) and gradient difference (GD) vectors (Figure 2) revealed the possibility of a [2+2] photocycloreversion process (involving the central moiety of TOD) for CI1 and a radical photocyclization for CI2, where the two interacting central carbon atoms are closer than the other

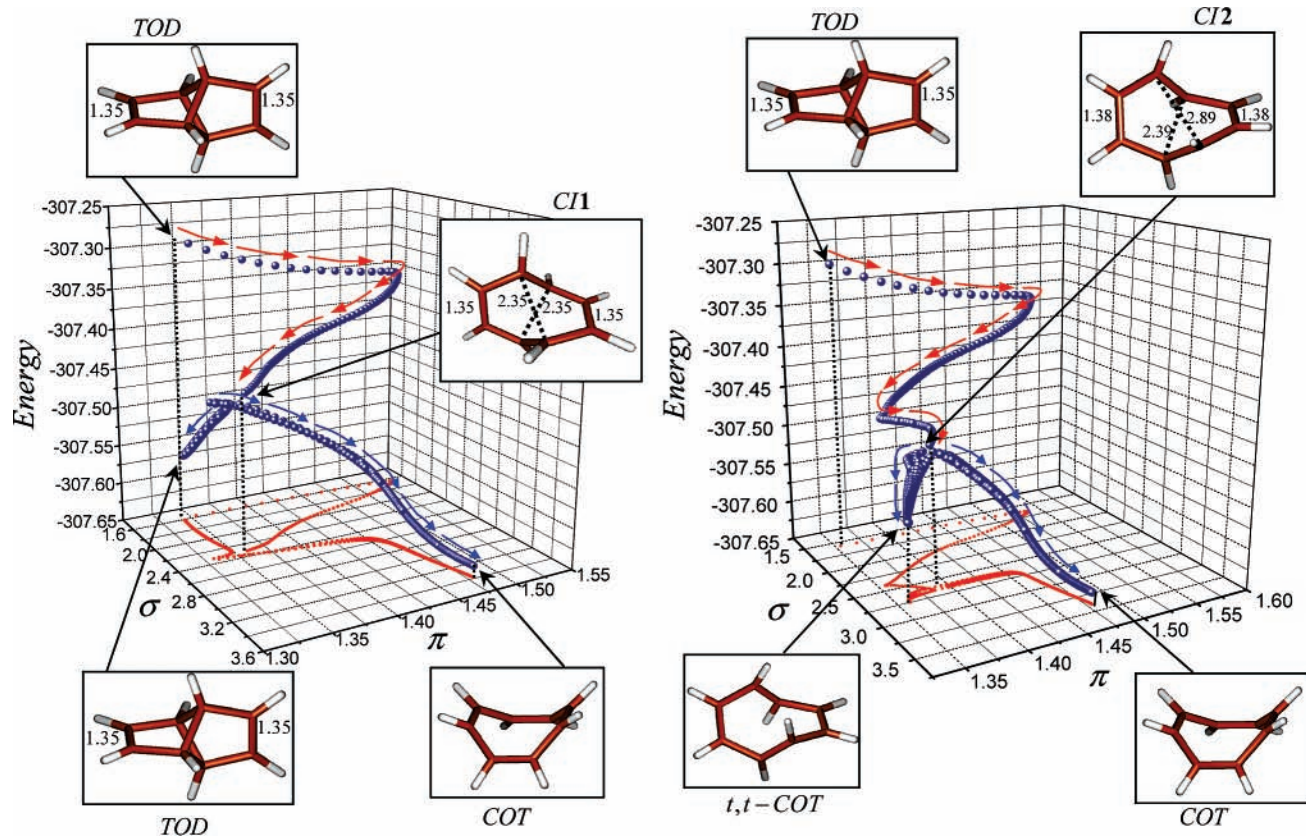


**Figure 3.** Energy (in au) profile of the complete relaxation process for the ultrafast photochemical reaction of TOD after the FC transition to  $S_1$  as a function of internal coordinates.<sup>9</sup> Relaxation on  $S_1$  (red arrows) allows the system to reach two different CIs (CI1 and CI2) of symmetry  $D_2$  (left) and  $C_2$  (right). The ultrafast decay to the ground state (blue arrows) via the conical intersections yield the formation of several photoproducts (TOD, COT, and *t,t*-COT).

two central atoms (see branching space diagrams in Figure 2; anyway, note that photocyclization from CI2 is aborted, as seen above).

The second type of TOD photochemical reaction pathway revealed by our MEP computations involves population of a biradical intermediate on  $S_1$  (**BR**)<sup>12</sup> (see Figure 1). In fact, the MEP associated with a distortion along the normal mode of symmetry  $C_s$  with imaginary frequency (see above), reaches an energy minimum (**BR**) with a biradical character on  $S_1$ . From **BR**, the system can reach, through three different transition states ( $TS_{CI3}$ ,  $TS_{CI4}$  and  $TS_{CI5}$ ) three new CIs (CI3, CI4 and CI5 of  $C_1$ ,  $C_s$ , and  $C_1$  symmetry respectively).

$TS_{CI3}$  is located  $\sim 15.5$  kcal/mol above **BR** at the CASSCF level of theory. Nevertheless, single-point CASPT2 correction to the energy along the computed IRC linking **BR** with CI3, leads to a flat transition state region, with only a  $\sim 4$  kcal/mol activation energy (see Table 1 and Figure 4). To better characterize **BR** and check if this is a real minimum or a non-stationary point, we have re-optimized this point using a CASPT2 numerical gradient with a CASSCF(6,6)/6-31G(d) zeroth-order wave function, including in the active space only the  $\pi$ -type molecular orbitals. A rapid convergence to a stationary point suggests that **BR** is a  $S_1$  minimum also at the CASPT2 level. On performing single-point correction at the improved CASPT2//CASSCF(8,8)/6-31G(d) level the energy of activation is corrected to an improved value of  $\sim 6$  kcal/mol (see Table 1).

Similar to CI3, also CI4 and CI5 are accessed from **BR** by overcoming a transition state on  $S_1$  ( $TS_{CI4}$  and  $TS_{CI5}$ , respectively). The energy profile along the MEP computed at the CASSCF level predicts 5.8 and 6.5 kcal/mol energy of activation

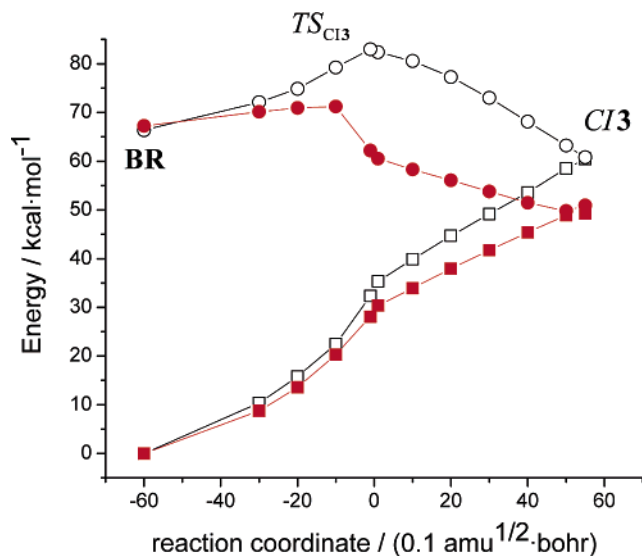


**Figure 4.** CASSCF IRC for  $TS_{CI3}$  and single-point CASPT2 correction to the energy. Filled symbols correspond to CASPT2 computations, while open symbols to CASSCF. Circles correspond to  $S_1$  state and squares to  $S_0$ . Relative energy in kcal/mol is referred to the  $S_0$  **BR** energy.

for the  $TS_{CI4}$  and  $TS_{CI5}$ , respectively. In order to obtain at least a qualitative value for the activation energy at the CASPT2 level of theory, we have performed a linear scan (in internal coordinates) from **BR** to CI4 and CI5. The results (see supporting material) predict a unique maximum along the path, with activation energies of 8.69 and 5.57 kcal/mol, respectively. Obviously, these values of energy of activation represent upper

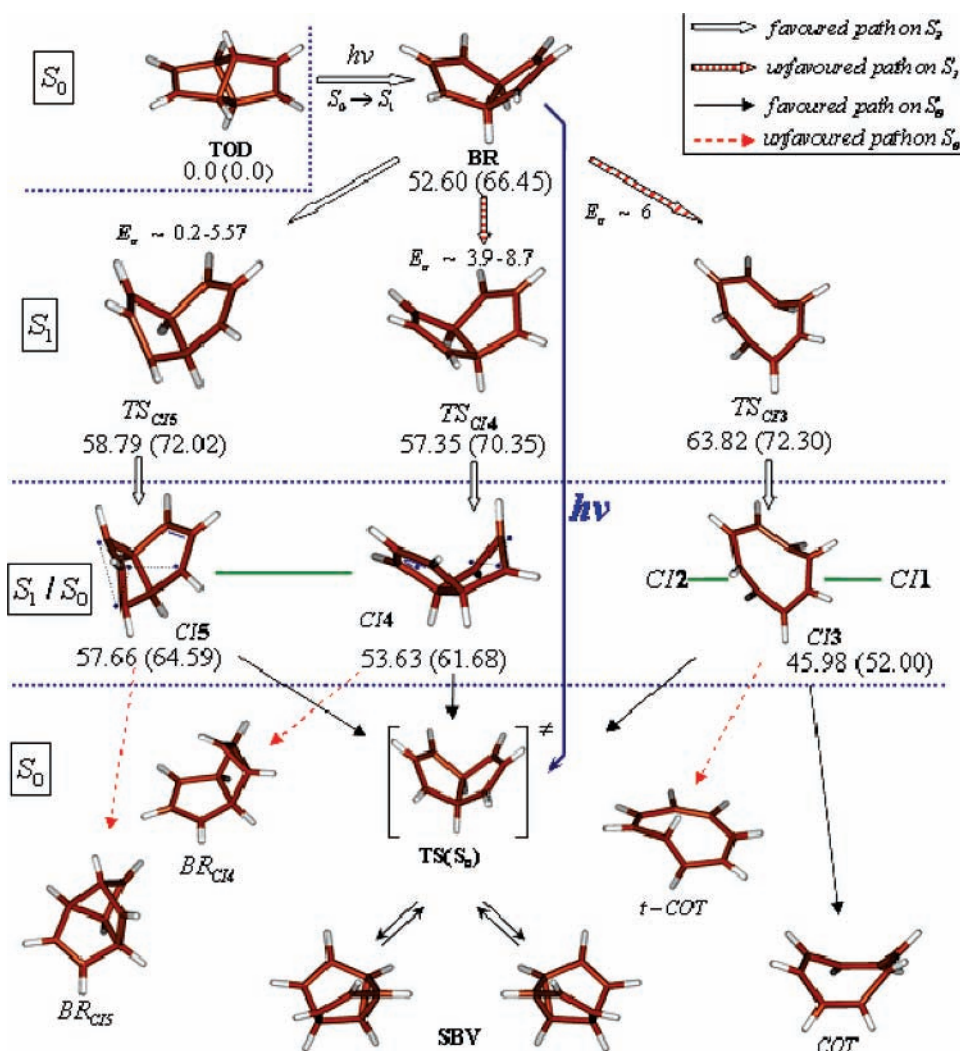


**Figure 5.** Photochemical processes for the second type of pathway of TOD via a BR on  $S_1$ . After the population of BR, three conical intersections (CI3, CI4, and CI5) can be reached by thermal activation, where the CASPT2 energies of activation ( $E_a$ ) are indicated. The favored and unfavored pathways on  $S_0$  and  $S_1$  are indicated. The intersection space is indicated by a continuous green line (linking CI1, CI2, and CI3 in one group and CI4 and CI5 in other). CASSCF energies for the optimized geometries are indicated, as well as CASPT2 single-point corrections (in brackets).

limits. Therefore, CASPT2 energies of activation are estimated by single-point corrections on the CASSCF transition state geometries with upper limits given by CASPT2 maxima along the scans. Consequently, the CASPT2 activation energies should be around 3.9 kcal/mol with an upper limit of 8.7 kcal/mol for  $TS_{CI4}$ , and around 0.2 kcal/mol with an upper limit of 5.6 kcal/mol for  $TS_{CI5}$ . In view of the small activation energies, we predict a short lifetime for BR, which will evolve along the three different pathways leading to CI3, CI4 and CI5. The accessibility of each pathway must be related to the corresponding activation energy; therefore, the efficiency should follow the order:  $TS_{CI5} > TS_{CI4} > TS_{CI3}$ . The MEP computed on  $S_0$  from the CIs<sup>10</sup> forms three different photoproducts. Thus, for CI3 the ~50% of the computed MEPs is related to the formation of COT, while ~40% is related to the formation of SBV and only ~10% is related to the formation of the t-COT isomer. Therefore, this CI3 seems to be an efficient channel to the formation of COT as well as SBV photoproducts, which are, as it has been noted before, the main photoproducts of the photochemical reaction. CI4 and CI5 are responsible for the formation of SBV, through the formation of a biradical structure on  $S_0$  with symmetry  $C_{2v}$  which corresponds to the transition state connecting two equivalent SBV in a Cope rearrangement process (Figure 5).<sup>13</sup> There is also the possibility

of forming other biradical species ( $BR_{CI4}$  and  $BR_{CI5}$ , see Figure 5) in the nonradiative decay through CI4 and CI5, due to  $\sigma$  bond formation. However, these channels for relaxation in the ground state are less favored compared with the formation of SBV because the accessibility of the valleys on the PES aids the formation of SBV, i.e., the beginning of the valley in the ground state PES associated with the formation of the biradical species,  $BR_{CI4}$  and  $BR_{CI5}$ , is more far from the cusp of the CI than that corresponding to the formation of the SBV. Thus, the valley for the formation of the biradical species  $BR_{CI4}$  is located at 0.2  $\text{amu}^{1/2}$  bohr,<sup>14</sup> while that corresponding to the formation of SBV is located at 0.02  $\text{amu}^{1/2}$  bohr from CI4. For CI5 the situation is analogous, the formation of the SBV being related to a path starting in the neighborhood of the CI (0.02  $\text{amu}^{1/2}$  bohr), while the path for the formation of the  $\sigma$  bond and the corresponding biradical species is located at 0.28  $\text{amu}^{1/2}$  bohr far away. Therefore, both CI4 and CI5 should be efficient funnels principally for the formation of SBV (and other biradical species to a minor extent).

The computed MEPs are in agreement with the main predictions that can be made from the analysis of the branching space for both CI4 and CI5 (see Figure 6). While this analysis provides a rationale for photoproducts formation,

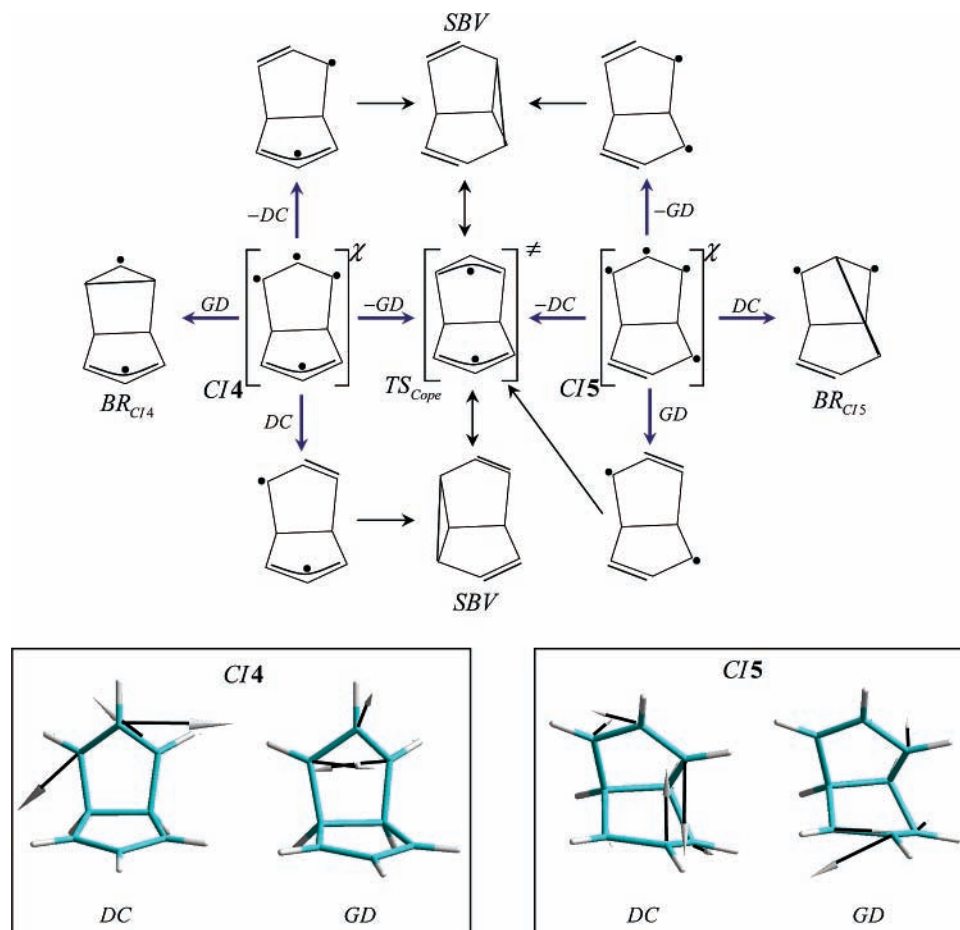


**Figure 6.** Branching space diagrams for CI4 and CI5. The DC and GD vectors for CI4 and CI5 of  $C_s$  and  $C_1$  symmetry are also shown.

only MEP computations tell us which photoproduct can be really formed.

Finally, it should also be possible for **BR** to decay radiatively to the ground state by forming the corresponding biradical structure on  $S_0$ . This biradical is close to the transition state structure for the Cope rearrangement interconverting two equivalent SBVs. Therefore, the formation of SBV is predicted by radiative decay to  $S_0$  through the **BR** intermediate on  $S_1$ . Moreover, this process is predicted to be a minor event due to the short lifetime expected for BR, as the small barrier to CI5 reveals.

In summary, for the second type of reaction pathway, a biradical species (**BR**) is populated in the  $S_1$  state. In both radiative and nonradiative decay processes to the ground state, the main photoproduct formed is the SBV, while COT can also be formed as a minor product in conjunction with t-COT and some biradical species.

**2. Intersection Space Analysis.** Using the conical intersection optimization method, we have been able to demonstrate the CI1, CI2, and CI3 converge to the same optimized conical intersection CIM (i.e., a stationary conical intersection point, featuring a vanishing gradient in the intersection space).<sup>15</sup> Therefore, the two immediately accessible CIs must belong to the same intersection space. In fact, during optimization the energy degeneracy is maintained, with the  $S_0$ – $S_1$  energy gap always  $< \sim 2.5$  kcal·mol<sup>-1</sup> and the step-size always low enough (maximum 0.1 bohrs or radians) to avoid discontinuity in the paths. This indicates that there is a continuous line of conical intersections connecting CI1, CI2, CI3, and CIM that, therefore, must belong to the same domain of a stationary CI.<sup>16</sup> Furthermore, we have been able to demonstrate that CIM pertains to

the intersection space in which a lower energy conical intersection (CIA) is contained. We have performed single-coordinate and double-coordinate relaxed scans in the  $S_1/S_0$  intersection space to prove that CIM and CIA are linked by a continuous space of intersection points (See Computational Details and Figure 7). The results indicate that CIM is a transition state in the intersection space and that a MEP on this space leads to the minimum CIA (See Figure 7). According to our previous works,<sup>17</sup> CIA (a conical intersection of symmetry  $C_{2v}$ ) is involved in the nonradiative decay process of excited COT. Indeed, CIA controls the photoinduced ring inversion and bond shifting of COT as well as the formation of two equivalent semibullvalene (SBV) photoproducts through a transition state for the Cope rearrangement.

Therefore, here we present an example in which different regions of the same continuous intersection space (i.e., the regions related with the stationary conical intersections CIA and CIM) provide diverse photochemical pathways for different valence isomers of the same compound (COT and TOD, respectively).

In common with CI1, CI2, CI3, CIM, and CIA, we have provided evidence that CI4 and CI5 belong to the same intersection space by locating a transition-state structure in the intersection space connecting both structures (see Supporting Information).

The analysis of the branching spaces associated with the two crossing seams suggests that these are not connected: in order to connect by a continuous hyperline the stationary conical intersections CIM with CI4 or CI5 it is necessary to form the central  $\sigma$  bond. The branching space for the CIM is qualitatively equal to that of the CI2 (see Figure 2), therefore any distortion

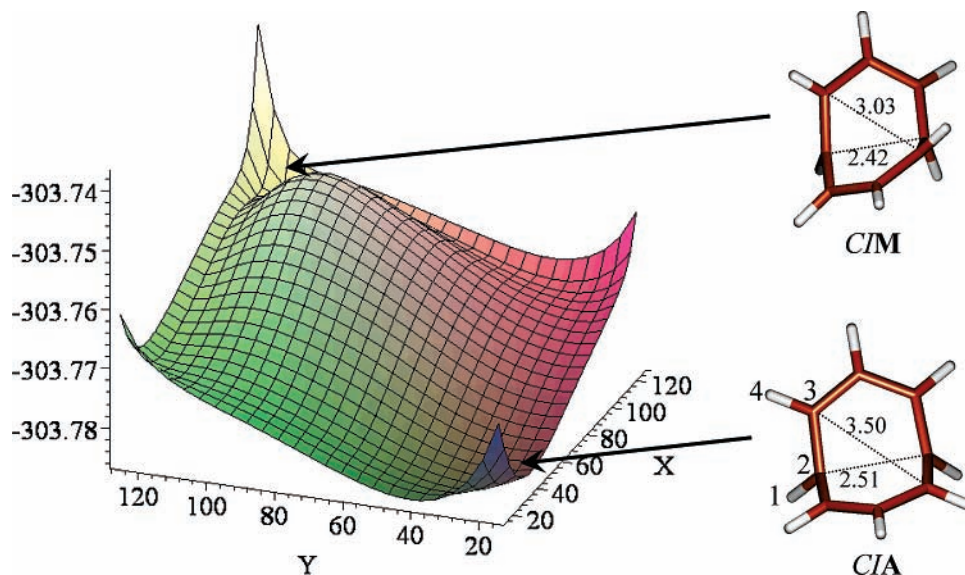


**Figure 7.** Relaxed double-coordinate scan (energies in a.u.) on the region of the intersection space linking the CIA and CIM conical intersections (see Computational Details). The surface was obtained by fitting a total of 1369 optimized points in the  $S_1/S_0$  intersection space to a polynomial function on “X” and “Y” with 55 parameters. The “X” and “Y” coordinates are given by the “1–2–3–4” dihedral angle and its  $C_2$  symmetry equivalent (where  $C_2$  symmetry is maintained for  $X=Y$ ).

used to form this central bond makes the molecule to leave the intersection space. Thus, it is very much unlikely that a continuous crossing seam exists connecting these two families of CIs, at least in the low-energy region of the intersection space.

### Computational Details

Most of the gradient computations (optimizations and minimum energy paths) were performed at the CASSCF(8e,8MO) level with a 6-31G(d) basis set. Analytical frequencies were performed at the same level of theory using the Gaussian98 suite of programs.<sup>18</sup> Single-point energy corrections at the CASPT2 level of theory and CASPT2 optimization of the **BR** structure using numerical gradients, were performed using the MOLCAS 6.0 suite of programs.<sup>19</sup> (Table 1)

The active space for the CAS calculation was chosen to include the hyperconjugation effect between the two double bonds through the cyclobutane central ring, by including  $\sigma$  orbitals of the central ring in the active space. The four  $\pi$ -type orbitals (2 occupied and the lowest 2 unoccupied), as well as four  $\sigma$ -type orbitals pertaining to the central cyclobutane ring were included in the active space. The  $\sigma$ -type orbitals are the lowest unoccupied and higher occupied and takes into account equal contribution of the four C atoms of the ring. Further single-point computations which include up to 12 electrons and 12 MO were performed to test the influence of the inclusion of all  $\sigma$  electrons for the central ring. No significant contributions of the new configurations respect to using the 8MO,8e scheme were found, which validates the selection of the 8MO,8e active space.

All the computed relaxation pathways (MEPs and initial relaxation directions) were performed at the CASSCF level of theory. In the  $S_1$  relaxation process the eigenvectors of the diagonalized Hessian matrix and the gradient vectors were taken as initial relaxation directions for computing the MEP. For the study of the relaxation process on  $S_0$  after passing through the funnel provided by the different conical intersections, twenty initial relaxation directions equally spaced in the branching space<sup>10</sup> were taken as initial relaxation directions. In addition, initial relaxation computations were performed to determine the

beginning of the valley corresponding to the formation of the photoproducts from the **CI4** and **CI5** conical intersections.<sup>14</sup>

Stationary points were fully optimized and characterized using analytical frequency calculations at the CASSCF level. The bifurcation points were located by diagonalizing the projected Hessian matrix<sup>20</sup> for every point along the MEP on  $S_1$ ; thus, the points of the MEP with closer to zero eigenvalues of the projected Hessian have been identified as bifurcation points. In the case of conical intersections, those involved in ultrafast processes (**CI1** and **CI2**) were determined by computing the state-averaged MEP on  $S_1$ , where the conical intersections are the final points of the corresponding MEP. The same situation is valid for **CI3**, **CI4**, and **CI5**, but here the MEP involves the associated transition state. The structures of **CI4** and **CI5** found with this procedure are virtually the same as those obtained from full optimizations in the intersection space by using standard methods of conical intersection optimizations as implemented in Gaussian98.<sup>18</sup> Finally, the relaxed scans involving **CIM** and **CIA** on the intersection space were performed at the CASSCF-(8e,8MO)/6-31G(d) level of theory for the single-coordinate, and due to the large number of optimizations (a total of 1369) the double-coordinate relaxed scan was performed at the CASSCF(8e,8MO)/STO-3G level using constrained optimizations in the intersection space.

### Conclusions

By constructing the branching space diagrams for the most representative conical intersections involved in the photochemistry of TOD (**CI1**, **CI2**, **CI4**, and **CI5**), we could account for the experimentally observed photoproducts (**COT** and **SBV**). These diagrams seem to be very useful in predicting the photochemical behavior of a chemical system, even for molecules showing complex photochemical behavior, as for TOD. Nevertheless, only by the analysis of the computed MEPs and relaxation processes both on the excited and the ground state, qualitative information on the efficiency and time scale for the process can be obtained. By performing different MEPs on  $S_1$ , we have found two bifurcation points. In particular, three main different minimum energy paths exist on  $S_1$ , which are related

to different photochemical processes. By following these MEPs, different conical intersection domains can be reached, which are related to different photochemical reactions and trigger the formation of the two main photoproducts: TOD and SBV. Because of the variety of the conical intersections involved in the decay to  $S_0$ , a deeper analysis of the intersection space was necessary to better understand the photoproduct formation. Thus, by carrying out the study of the topology of the intersection space as well as the related relaxation paths on  $S_0$ , we have found that the simple low lying intersection space domain including CI1, CI2, and CI3 (as well as CIA, which is related to COT photochemistry) is responsible for COT formation. Since this segment of intersection space is directly accessible via barrierless routes on  $S_1$ , we expect COT formation to be efficient and ultrafast, as well as the main photoproduct afforded by the photochemical reaction, in agreement with the experiments. Similarly, a second intersection space domain has been located (including CI4 and CI5) which is unconnected to the first and mediates SBV photoproduct formation through barrier (although small) controlled paths (i.e., longer time-scales), thus affording the secondary photoproduct. Therefore, the two intersection space domains which are “chemically” distinct, are related to the formation of the two main photoproducts in a different time-scale: COT (involving an ultrafast—barrierless—process) and SBV (involving an excited-state biradical intermediate and a barrier activated process). Together with the formation of COT, the first intersection space domain is responsible for the back formation of TOD and t,t-COT to a minor extent, which at room temperature should isomerize to yield the most stable conformation: COT. Moreover, there are qualitative differences between the conical intersections belonging to this intersection space, since CI1 corresponds with a [2+2] cycloaddition while CI2 formally corresponds with a photocyclization process (although this is aborted).

In contrast, the second type of photochemical behavior implies the population of a relatively unstable biradical intermediate on  $S_1$  (BR). From this intermediate, it is possible to reach two different CIs belonging to the same segment of the intersection space. These CIs (CI4 and CI5), in addition to providing a route for radiationless decay and SBV formation, may also be responsible to the formation (to a minor degree) of other biradicals.

In conclusion, the experimentally detected photochemical products SBV and COT are correctly predicted to be formed in a different amount and in different time-scales (ultrafast for the primary COT product, and via a slower biradical-mediated process for the secondary SBV product) and involve different conical intersections which belong to different intersection space domains.

**Acknowledgment.** This work is dedicated to the memory of Professor Fernando Bernardi. The authors thank Dr. Raúl Palmeiro for providing the program for determining the BPs on  $S_1$ . Work financed by Projects BQU2003-07281 and CTQ2006-07643 from the Spanish Ministry of Education and Science and project CAM-UAH2005/037 of the Autonomous Community of Madrid and University of Alcalá. L.M.F. acknowledges the Spanish Ministry of Education and Science for a postdoctoral grant (ref EX-2005-0454). U.S. is grateful to the Council of Education of Madrid and to the European Social Fund for a doctoral fellowship.

**Supporting Information Available:** Cartesian coordinates, transition state structure, and scans from BR to CI4 and CI5.

This material is available free of charge via the Internet at <http://pubs.acs.org>.

## References and Notes

- (1) (a) For a recent review, see: Migani, A. and Olivucci, M. In *Conical Intersections. Electronic Structure, Dynamics and Spectroscopy*; Domcke, W., Yarkony, D. R., Köppel, H. Eds.; World Scientific: Singapore, 2004. (b) Olivucci, M. and Sinicropi, A. In *Computational Photochemistry*; Olivucci, M. Ed.; Elsevier: Amsterdam, 2005; Vol. 16. (c) Garavelli, M. *Theor. Chem. Acc.* **2006**, *116*, 87–105.
- (2) See for example: (a) Salem, L. *Electrons in Chemical Reactions: First Principles*; Wiley: New York, 1982, pp 149–151. (b) Klessinger M, Michl J. *Excited States and Photochemistry of Organic Molecules*; VCH Publishers: New York, 1994.
- (3) See, for example (a) Migani, A.; Robb, M. A.; Olivucci, M. J. *Am. Chem. Soc.* **2003**, *125*, 2804–2808. (b) Frutos, L. M.; Sancho, U.; Castaño, O. *Org. Lett.* **2004**, *6*, 1229–1231. (c) Cembran, A.; Bernardi, F.; Garavelli, M.; Gagliardi, L.; Orlandi, G. *J. Am. Chem. Soc.* **2004**, *126*, 3234–3243.
- (4) Meinwald, J.; Tsuruta, T. *J. Am. Chem. Soc.* **1970**, *92*, 2579.
- (5) (a) Gleiter, R.; Kobayashi, T. *Helv. Chim. Acta* **1971**, *54*, 1081. (b) Bischof, P.; Gleiter, R.; Haider, R. *Angew. Chem., Int. Ed. Engl.* **1977**, *16*, 110. (c) Kanda, K.; Koremoro, T.; Imamura, A. *Tetrahedron* **1986**, *42*, 4169.
- (6) A total of 8e, 8MO has been chosen for the active space, corresponding to 4e, 4MO for the two double bonds ( $\pi$  orbitals) and 4e, 4MO (two first HOMOs and two first LUMOs) for the central cyclobutane ring ( $\sigma$  orbitals).
- (7) The negative eigenvalues of the Hessian matrix determined for the FC geometry on  $S_1$  are  $-844$ ,  $-761$ ,  $-593$  ( $\times 2$ ) and  $-322$   $\text{cm}^{-1}$  with symmetries  $D_2$ ,  $C_2$ ,  $C_s$  (2-fold), and  $D_2$  respectively. The corresponding eigenvectors, which were all orthogonal to the gradient, give the direction of energy decrease within a second order approximation for the PES around the FC geometry on  $S_1$ .
- (8) These five directions provide a five-dimensional subspace of energy decreases in a second order approximation, while the orthogonal force (i.e., minus energy gradient) vector provides a first-order decrease in the energy. Therefore, any linear combination of these six vectors gives a six-order dimensional subspace of potential energy decrease within first- and second-order expansion of the PES.
- (9) The sigma ( $\sigma$ ) coordinate corresponds with the average value of the length for the two opposite  $\sigma$  CC bonds of the central cyclobutane ring which are broken in the relaxation process on  $S_1$  (e.g.,  $C_1-C_2$  and  $C_5-C_6$ ). The pi ( $\pi$ ) coordinate stands for the average value of the length for the CC double bonds (i.e.,  $C_3=C_4$  and  $C_7=C_8$ ).
- (10) 20 MEPs in  $S_0$  were computed for every CI, taking as initial direction to follow the corresponding 20 equally spaced vectors (0.1 $\pi$  radians) belonging to the plane defined by the gradient difference (GD) and derivative coupling (DC) vectors of each CI.
- (11) Unless the experimentally observed photoproducts (SBV and COT) in an approximate ratio of 1:2) are involved, the formation of structural isomers of COT which rapidly isomerize to COT is not excluded, even at temperatures as low as  $-60$  °C. See ref 4.
- (12) The BR intermediate on  $S_1$  has biradical character, but with a contribution from a tetradical form.
- (13) (a) Cheng, A. K.; Anet, F. A. L.; Mioduski, J.; Meinwald, J. *J. Am. Chem. Soc.* **1974**, *96*, 2887. (b) Castano, O.; Frutos, L.-M.; Palmeiro, R.; Notario, R.; Andres, J.-L.; Gomperts, R.; Blancafort, L.; Robb, M. A. *Angew. Chem., Int. Ed.* **2000**, *39*, 2095. (c) Jiao, H. J.; Nagelkerke, R.; Kurtz, H. A.; Williams, R. V.; Borden, W. T.; Schleyer, P. V. *J. Am. Chem. Soc.* **1997**, *119*, 5921.
- (14) Due to the relatively large distance between C atoms for the formation of the C–C bonds in CI4 and CI5 to yield BR<sub>CI4</sub> and BR<sub>CI5</sub>, we have located the distance (from the tip of the CI) of the beginning of the corresponding valley on the ground state for each photoproduct (i.e., BR<sub>CI4</sub> and BR<sub>CI5</sub> and SBV). This is an index of the relative accessibility of each relaxation process. In practice, this distance has been computed by incrementing the initial relaxation direction displacement for MEPs computation by steps of 0.02  $\text{amu}^{1/2}$  bohr units from both CI4 and CI5.
- (15) By performing MEP computations in the intersection subspace (with a standard conical intersection optimization algorithm as implemented in the Gaussian suite of programs. See ref 18), CIM has been located from CI1 and CI2.
- (16) By a domain of a stationary CI (i.e., vanishing gradient in the intersection space) we mean a continuous subspace of CIs in which the stationary CI is included. This implies that, for every CI point of this subspace, a MEP exists in the intersection space that connects that point to the stationary CI.
- (17) (a) Garavelli, M.; Bernardi, F.; Moliner, V.; Olivucci, M. *Angew. Chem., Int. Ed.* **2001**, *40*, 1466. (b) Garavelli, M.; Bernardi, F.; Cembran, A.; Castaño, O.; Frutos, L. M.; Merchán, M.; Olivucci, M. *J. Am. Chem. Soc.* **2002**, *124*, 13770.

(18) Calculations were made with: Frisch, M. J.; Trucks, G. W.; Schlegel, H. B.; Scuseria, G. E.; Robb, M. A.; Cheeseman, J. R.; Zakrzewski, V. G.; Montgomery, J. A., Jr.; Stratman, R. E.; Burant, J. C.; Dapprich, Millam, S. J. M.; Daniels, A. D.; Kudin, K. N.; Strain, M. C.; Farkas, O.; Tomasi, J.; Barone, V.; Cossi, M.; Cammi, R.; Mennucci, B.; Pomelli, C.; Adamo, C.; Clifford, S.; Ochterski, J.; Petersson, G. A.; Ayala, P. Y.; Cui, Q.; Morokuma, K.; Malick, D. K.; Rabuck, A.; Raghavachari, D. K.; Foresman, J. B.; Cioslowski, J.; Ortiz, J. V.; Stefanov, B. B.; Liu, G.; Liashenko, A.; Piskorz, P.; Komaromi, I.; Gomperts, R.; Martin, R. L.; Fox, D. J.; Keith, T.; Al-Laham, M. A.; Peng, C. Y.; Nanayakkara, A.; Gonzalez, C.; Challacombe, M.; Gill, P. M. W.; Johnson, B. G.; Chen, W.; Wong, M. W.; Andres, J. L.; Gonzalez, C.; Head-Gordon, M.; Replogle,

E. S.; Pople, J. A. *Gaussian 98*, Revision A.7; Gaussian, Inc.: Pittsburgh PA, 1998.

(19) Calculations were made with: Andersson, K.; Barysz, M.; Bernhardsson, A.; Blomberg, M. R. A.; Carissan, Y.; Cooper, D. L.; Fülscher, M. P.; Gagliardi, L.; de Graaf, C.; Hess, B. A.; Hagberg, D.; Karlström, G.; Lindh, R.; Malmqvist, Nakajima, P.-Å.; T.; Neogrády, P.; Olsen, J.; Raab, J.; Roos, B. O.; Ryde, U.; Schimmelpfennig, B.; Schütz, M.; Seijo, L.; Serrano-Andrés, L.; Siegbahn, P. E. M.; Ståhring, J.; Thorsteinsson, T.; Veryazov, V.; Widmark, P.-O. *MOLCAS*, version 6; Lund University: Lund, Sweden, 2004.

(20) Algorithm taken from: Palmeiro, R. Ph.D. Dissertation, University of Alcalá, Spain, 2004.